Journal of Theoretical and Applied Mechanics, Sofia, Vol.55 (2025) pp. 402-415
FLUID MECHANICS

AN APPROXIMATE SOLUTION FOR THE FLOW OVER A FINITE SINUSOIDAL OBSTACLE WITH A HIGH WEBER NUMBER EFFECT AND ZERO GRAVITY

MAY MANAL BOUNIF[1], ABDELKADER GASMI[2*]

[1]*Higher School of Management and Digital Economy, Kolea, Algeria*
[2]*Laboratory of Pure and Applied Mathematics, Faculty of Mathematics and Informatics, University of M'sila, Algeria*

[Received: 10 April 2025. Accepted: 30 September 2025]
doi: https://doi.org/10.55787/jtams.25.55.4.402

ABSTRACT: This paper considers the problem of inviscid and incompressible flow with a free surface over sinusoidal obstacles of finite length placed in the bottom with finite length. The flow is considered by neglecting the gravity effect, but we take into account the surface tension effect. Applying the first order perturbation technique in conjunction with the Hilbert transformation, we provide an approximate solution to the boundary value problem with mixed boundary conditions arising from the flow problem. The unknown free-surface profiles are established for each large value of the Weber number. The obtained results reveal the simplicity of the used method; they also provide approximate solutions to these kinds of problems.

KEY WORDS: Free surface, flow, surface tension, Hilbert method, perturbation technique.

1 INTRODUCTION

Modeling marine sciences related physical phenomena has been a subject of extensive research over the years. This study aims to investigate the problem of free surface flow of inviscid and incompressible fluid over given's obstacles. The problem of free-surface flow of inviscid and incompressible fluids over various bottom topographies has received considerable attention due to its relevance in predicting the quality and shapes of submerged bodies. This problem is classified among the flows that study the effect of immersed bodies on free surfaces, for more details related to this subject see for example Birkhoff and Zarantonello [1], Batchelor [2] Bhimsen and Shivamoggi [3], Milne-Thomson [4] and Rutherford [5].

Several mathematical techniques have been employed to study free-surface flows over obstacles of varying geometries. Forbes and Schwartz [6] tackled the flow over

*Corresponding author e-mail: abdelkader.gasmi@univ-msila.dz

a semi-circular obstruction using integrodifferential equations. Similarly, Vanden-Broeck [7] analyzed the same problem numerically and discussed the existence of supercritical solutions. Dias et al. [8] considered the flow over rectangular weirs and calculated the discharge coefficient for weirs of different heights and lengths. Bounif and Gasmi [9, 10], Mina and Hanna [11], on the other hand, examined the problem that involves a free-surface flows over a step at the bottom of a channel, they offered a solution to the problem using the perturbation method. As we can also consider the proposed problem belongs to the class of flow over a corrugated topography, you can see, for example Keeler et al. [12] explored the flow over a corrugated topography using both weakly nonlinear and fully nonlinear models,They classified solutions in terms of a depth-based Froude number and the four classical flow types (supercritical, subcritical, generalized hydraulic rise, and hydraulic rise) for flow over a small bump.

Despite these advancements, the flow over a sinusoidal obstacle of finite length with surface tension effects remains relatively unexplored. The consideration of sinusoidal bottoms can be crucial since they are a naturally occurring phenomenon in valleys and rivers, as well as seas in which they form due to sedimentation of sand forming ripples. This study focuses on the incompressible and inviscid flow over sinusoidal bottoms. The mathematical formulation is derived as a mixed boundary value problem (BVP). To solve this BVP approximately, first-order perturbation techniques are combined with the Hilbert transformation.

The structure of this paper is as follows: Section 2 presents the mathematical formulation of the problem. Then Section 3 derives the approximate equations. Section 4 outlines the application of first-order perturbation techniques to obtain solutions. Section 5 discusses the results and includes streamline profiles before concluding the study.

2 Mathematical Formulation

Let us consider the motion of a two-dimensional flow over sinusoidal obstacle of finite length placed in the bottom ($\delta(x) = \sin(ax)/b$). We assume that the fluid is incompressible, irrotational and inviscid. We also consider the effect of the superficial tension while we neglect the effect of gravity.

Under the assumption of irrotationnality, the flow of incompressible fluids can be governed by Laplace's equation for the velocity potential φ

$$\Delta\varphi = 0, \tag{1}$$

the complex potential $f = \varphi + i\psi$, where ψ is the stream function, is an analytical function of $z = x + iy$ in the flow region. Its derivative, the complex conjugate of

the velocity, is given by:

$$\xi = \frac{df}{dz} = u - iv = qe^{-i\theta}, \tag{2}$$

where q is the flow speed, θ is the velocity vector's inclination angle, and u, v are the velocity components,

$$\begin{cases} u = \dfrac{\partial \varphi}{\partial x} = \dfrac{\partial \psi}{\partial y}, \\ v = \dfrac{\partial \varphi}{\partial y} = -\dfrac{\partial \psi}{\partial x}. \end{cases} \tag{3}$$

Far upstream and downstream, the flow is proposed as uniform with constant flux: $U_1 h_1 = U_2 h_2$, where , $U_i, i = 1, 2$ and $h_i, i = 1, 2$ are velocities and depths of the flow upstream and downstream, respectively. The bottom consists of a horizontal plane C_0C_1, an obstacle described by $(\delta(x) = \sin(ax)/b)$, $x \in [0, n\pi/a], n = 1, 2, 3, \ldots$, and a horizontal plane C_NC_∞, where the bottom extends from $-\infty$ (point C_0) to $+\infty$ (point C_∞). Hence, we choose the point C_1 as the origin in the z-plane (see Fig. 1).

The length of the obstacle is:

$$\|C_1C_N\| = L_n = \frac{n\pi}{a}, n = 1, 2, 3, \ldots. \tag{4}$$

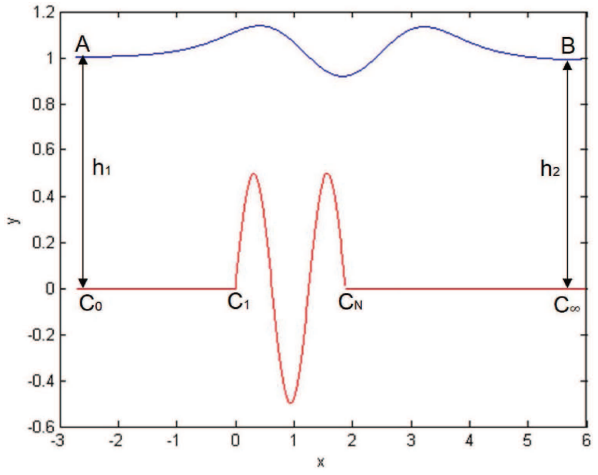

Fig. 1. Sketch of the flow and of the coordinates. The figure shows a computed surface profile for $\delta(x) = \sin(5x)/2$, the periodic $n = 3$ and $N = 420$.

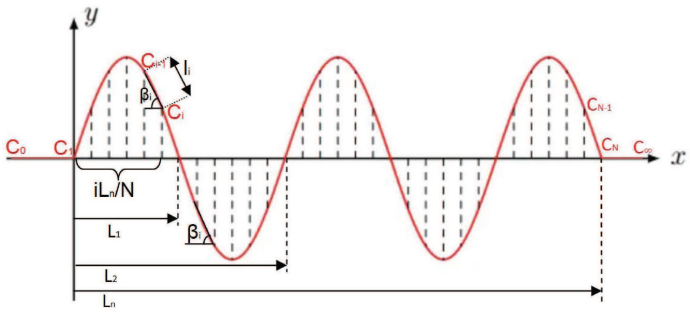

Fig. 2. Discretization of a sinusoidal bottom.

This length is discretized into N mesh points $C_i, i = 1, 2, \ldots, N$, with inclination angles between segments C_iC_{i+1} and the horizontal given by:

$$\beta_i = \arccos\left(\frac{L_n}{Nl_i}\right); \quad i = 1, \ldots, N-1, \tag{5}$$

where

$$l_i = \|C_iC_{i+1}\| = \sqrt{\left(\frac{L_n}{N}\right)^2 + \left(\delta\left(\frac{(i+1)L_n}{N}\right) - \delta\left(\frac{iL_n}{N}\right)\right)^2}. \tag{6}$$

The dimensionless variables are defined by choosing U as the reference velocity and $h_1$as the reference length.

Let

$$\kappa = \ln \xi = \ln q - i\theta, \tag{7}$$

we call κ a logarithmic hodograph variable. It follows from (2)and (7) that:

$$z = \int e^{-\kappa} df. \tag{8}$$

We choose $\varphi = 0$ at a point C_1 and $\psi = 1$ on the streamline AB, $\psi = 0$ on the streamline $C_0C_1 \ldots C_NC_\infty$ (see figure 3).

From Gasmi [13], on the free-surface AB, where the pressure is uniform, the Bernoulli's condition is given by:

$$\frac{1}{2}(\varphi_x^2 + \varphi_y^2) + \frac{P}{\rho} = \frac{1}{2}U_1^2 + \frac{P_0}{\rho}, \tag{9}$$

where ρ is the density, P is the fluid pressure beneath the free surface and P_0 is the atmospheric pressure. The right-hand side of equation (9) is evaluated from the condition far downstream.

Using Laplace's formula

$$P - P_0 = KT,$$

where T is the surface tension and K is the curvature.

Dimensionless variables are introduced using a reference velocity U_1 and reference length h_1. Under these conditions, equation (9) becomes:

$$(\varphi_x^2 + \varphi_y^2) + 2\frac{T}{h_1 U_1^2 \rho} K = 1,$$

and as we have

$$ds = \sqrt{dx^2 + dy^2},$$

we can write the previous equationas follows

$$(\frac{d\varphi}{ds})^2 + \frac{2}{\sigma}\frac{d\theta}{ds} = 1, \tag{10}$$

where $\sigma = \frac{h_1 U_1^2 \rho}{T}$ is the Weber number. Using the Schwartz-Christoffel transformation, we map the flow in the physical plane in f-plane (in Fig. 3) onto the upper half

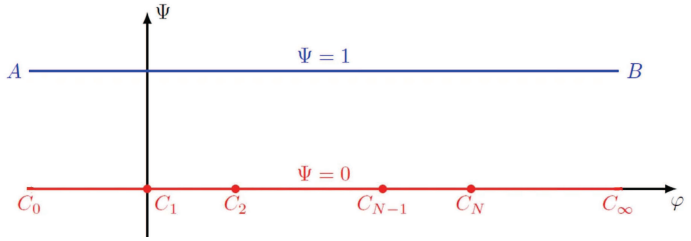

Fig. 3. The potential f plane.

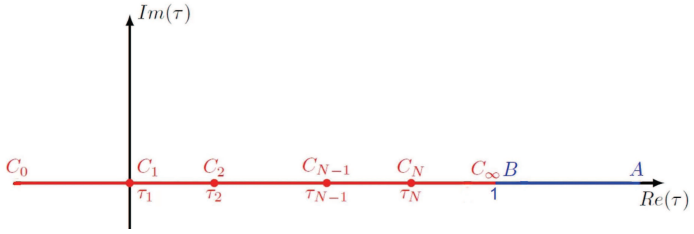

Fig. 4. The auxiliary plane.

of an auxiliary τ-plane (in Fig. 4). The resulting transformation is the following:

$$f(\tau) = -\frac{1}{\pi}\ln(1-\tau), \quad 0 < \arg(\tau - 1) < \pi \tag{11}$$

After applying the Hilbert method for a mixed boundary-value problem in the t-plane, for $\tau > 1$ and for $n = 1, 2, 3, \ldots$, we have the following system of the nonlinear integral equations:

$$\theta(\tau) = \frac{\sqrt{\tau-1}}{\pi}\left\{p.v.\int_1^{+\infty}\frac{\ln q(s)}{(s-\tau)\sqrt{(s-1)}}ds\right\} + \sum_{i=1}^{N/2n} I_i(\tau) - \sum_{k=0}^{n-1}(-1)^k \sum_{i=(2k+1)N/2n}^{(2k+3)N/2n} I_i(\tau) + (-1)^n \sum_{i=(2n-1)N/2n}^{N-1} I_i(\tau), \tag{12}$$

where

$$I_i(\tau) = -\frac{\sqrt{\tau-1}}{\pi}\int_{\tau_i}^{\tau_{i+1}}\frac{\beta_i}{(s-\tau)\sqrt{(1-s)}}ds, \quad i = 1, 2, \ldots, N-1, \tag{13}$$

$$= \frac{2\beta_i}{\pi}\tan^{-1}\left(\frac{\left(\sqrt{1-\tau_i} - \sqrt{1-\tau_{i+1}}\right)\sqrt{(\tau-1)}}{\tau - 1 + \sqrt{(1-\tau_i)\,(1-\tau_{i+1})}}\right).$$

Using (8) and (11) the coordinates of a point on the free-surface can be obtained as follows:

$$z(\tau) = z_\infty - \frac{1}{\pi}\int_\tau^{+\infty}\frac{e^{i\theta(s)}}{(1-s)q(s)}ds, \quad \tau > 1, \tag{14}$$

Separating the real and imaginary parts, we get:

$$x(\tau) = x_\infty - \frac{1}{\pi}\int_\tau^{+\infty}\frac{\cos\theta(s)}{(1-s)q(s)}ds, \ \tau > 1, \tag{15}$$

$$y(\tau) = 1 - \frac{1}{\pi}\int_\tau^{+\infty}\frac{\sin\theta(s)}{(1-s)q(s)}ds, \ \tau > 1. \tag{16}$$

3 The Approximate Equations

In this section, we approximate the nonlinear integral equations (9),(12),(15) and (16), when the Weber number σ is large.

By using the first-order Taylor development with respect to $\frac{1}{\sigma}\left|\frac{\partial\theta}{\partial\varphi}\right|$, the solution of the Bernoulli equation (9)is given by

$$q(t) \approx 1 - \frac{1}{\sigma}\left|\frac{\partial\theta}{\partial\varphi}\right|, \tag{17}$$

Using relation (11), we obtain:

$$\frac{\partial\theta}{\partial\varphi} = \frac{\partial\theta}{\partial\tau}\frac{\partial\tau}{\partial\varphi} = \pi(\tau-1)\frac{\partial\theta}{\partial\tau}, \quad \tau > 1. \tag{18}$$

Consequently, for $\tau > 1$, we approximate the flow speed by:

$$q(\tau) \approx 1 - \frac{\pi}{\sigma}(\tau-1)\frac{\partial\theta}{\partial\tau}(\tau), \tag{19}$$

which yields

$$\ln q(\tau) \approx -\frac{\pi}{\sigma}(\tau-1)\frac{\partial\theta}{\partial\tau}(\tau), \tag{20}$$

and

$$\frac{1}{q(\tau)} \approx 1 + \frac{\pi}{\sigma}(\tau-1)\frac{\partial\theta}{\partial\tau}(\tau), \tag{21}$$

For small angles β_i, the change in θ will be minor, thus, allowing us to approximate $\sin\theta$ by $\theta(t)$ and $\cos\theta$ by one.

Using (20), we can approximate the angle of the free surface with the horizontal (12) by

$$\begin{aligned}\theta(\tau) \approx -\frac{\sqrt{t-1}}{\sigma} p.v. \int_1^{+\infty} \frac{(s-1)\theta'(s)}{(s-\tau)\sqrt{s-1}} ds + \sum_{i=1}^{N/2n} I_i(\tau) \\ - \sum_{k=0}^{n-1} (-1)^k \sum_{i=(2k+1)N/2n}^{(2k+3)N/2n} I_i(\tau) + (-1)^n \sum_{i=(2n-1)N/2n}^{N-1} I_i(\tau).\end{aligned} \tag{22}$$

Substituting (21) into (15) and (16), and after simplification, the free surface equations take the form:

The real part,

$$\begin{aligned} x(\tau) &\approx x_\infty - \frac{1}{\pi}\int_\tau^{+\infty} \frac{1}{(1-s)}\left[1 + \frac{\pi}{\sigma}(s-1)\theta'(s)\right] ds, \\ &\approx x_\infty - \frac{1}{\pi}\int_\tau^{+\infty} \frac{1}{(1-s)} ds + \frac{1}{\sigma}\left[\lim_{s\longrightarrow\infty}\theta(s) - \theta(\tau)\right], \\ &\approx x_\infty - \frac{1}{\pi}\int_\tau^{+\infty} \frac{1}{(1-s)} ds - \frac{1}{\sigma}\theta(\tau). \end{aligned} \tag{23}$$

The imaginary part,

$$y(\tau) \approx 1 - \frac{1}{\pi}\int_{\tau}^{+\infty} \frac{\theta(s)}{(1-s)}\left[1 + \frac{\pi}{\sigma}(s-1)\theta^{'}(s)\right] ds, \tag{24}$$

$$\approx 1 - \frac{1}{\pi}\int_{\tau}^{+\infty} \frac{\theta(s)}{(1-s)} ds + \frac{1}{2\sigma}\left[\lim_{s\longrightarrow\infty} \theta^2(s) - \theta^2(\tau)\right],$$

$$\approx 1 - \frac{1}{\pi}\int_{\tau}^{+\infty} \frac{\theta(s)}{(1-s)} ds - \frac{\theta^2(\tau)}{2\sigma}.$$

To solve the system of the nonlinear integral equations (19), (22)–(24), we use the Perturbation technique.

4 Perturbation Technique

We can expand $X(\tau)$ by means of small parameters β_i that correspond to the tangent angles, thus, we get:

$$X(\tau) = \sum_{i=1}^{N}\sum_{j=0}^{\infty} \beta_i^j X_{j,\beta_i}(\tau). \tag{25}$$

Here $X(\tau)$ stands for $q(\tau), \theta(\tau), \theta^{'}(\tau), x(\tau)$and $y(\tau)$.

4.1 Zero-order approximation

The respective case conforms with the flow far upstream, which we regard as uniform. Consequently, the zero-order approximation of the nonlinear integral equations (19), (22)-(24), is presented by:

The velocity of the flow

$$q_0(\tau) \approx 1 - \frac{\pi}{\sigma}(\tau-1)\theta_0^{'}(\tau) \approx 1. \tag{26}$$

Therefore, the velocity direction relative to the horizontal axis is presented as:

$$\theta_0(\tau) \approx -\frac{\sqrt{\tau-1}}{\sigma} p.v. \int_{1}^{+\infty} \frac{\sqrt{s-1}\theta_0^{'}(s)}{(s-\tau)} ds \approx 0. \tag{27}$$

And the free streamline equations:

$$x_0(\tau) \approx x_\infty - \frac{1}{\pi}\int_{\tau}^{+\infty} \frac{1}{(1-s)} ds - \frac{1}{\sigma}\theta_0(\tau) \tag{28}$$

$$\approx x_\infty - \frac{1}{\pi}\int_{\tau}^{+\infty} \frac{1}{(1-s)} ds.$$

and

$$y_0(\tau) \approx 1 - \frac{1}{\pi}\int_{\tau}^{+\infty} \frac{\theta_0(s)}{(1-s)}ds - \frac{\theta_0^2(\tau)}{2\sigma} \approx 1. \tag{29}$$

On the other hand, we have the formula:

$$x_\infty \approx \frac{1}{\pi} p.v. \int_0^{+\infty} \frac{1}{(1-s)}ds, \tag{30}$$

hence

$$x_0(t) \approx -\frac{1}{\pi}\ln(\tau - 1). \tag{31}$$

4.2 First-order approximation

Now, we find the first-order approximation of the nonlinear integral equations (19), (22)-(24). To reach this end, we use development (25) and the zero-order approximation of the system.

Using the development (25), we can write

$$X_{1,\beta_i}(\tau) \approx \frac{X(\tau) - X_0(\tau)}{\beta_i}. \tag{32}$$

By substituting (19) and (26) into (32), we get the first-order approximation of the flow speed:

$$q_{1,\beta_i}(\tau) \approx -\frac{\pi}{\sigma}(\tau - 1)\theta'_{1,\beta_i}(\tau). \tag{33}$$

Then, using (22), (27) and (32), the first-order approximation of the inclination of the velocity vector takes the form:

$$\theta_{1,\beta_i}(\tau) \approx -\frac{\sqrt{\tau - 1}}{\sigma} p.v. \int_1^{+\infty} \frac{(s-1)\theta'_{1,\beta_i}(s)}{(s-\tau)\sqrt{s-1}}ds + I_i(\tau)\Upsilon_{k,i}. \tag{34}$$

On the other hand, from (23), (31) and (32), we find:

$$x_{1,\beta_i}(\tau) \approx -\frac{1}{\sigma}\theta_{1,\beta_i}(\tau). \tag{35}$$

Then, using (24), (29) and (32), we have

$$y_{1,\beta_i}(\tau) \approx -\frac{1}{\pi}\int_{\tau}^{+\infty} \frac{\theta_{1,\beta_i}(s)}{(1-s)}ds. \tag{36}$$

Where $I_i(\tau)$ is defined in (13) and

$$\Upsilon_{k,i} = \begin{cases} \frac{1}{\beta_i}; & 1 < i < N/2n \\ -\frac{(-1)^K}{\beta_i}; & \frac{(2k+1)N}{2n} < i < \frac{(2k+3)N}{2n}, 0 < k < n-1, \\ \frac{(-1)^n}{\beta_i}; & \frac{(2n-1)N}{2n} < i < N-1, \end{cases} \tag{37}$$

From (34), and for a very large value of the Weber number σ, we may neglect the first term with respect to the second one. Thus, we get the first-order approximation of the velocity direction relative to the horizontal axis:

$$\theta_{1,\beta_i}(\tau) \approx I_i(\tau)\Upsilon_{k,i}, \quad \tau > 1. \tag{38}$$

Substituting (38) into (35) and (36) and carrying out the integration, we find the first-order approximation of the free streamlines:

$$y_{1,\beta_i}(\tau) \approx \begin{cases} J_i(\tau); & 1 < i < \frac{N}{2n}, \\ -(-1)^k J_i(\tau); & \frac{(2k+1)N}{2n} < i < \frac{(2k+3)N}{2n}, 0 < k < n-1, \\ (-1)^n J_i(\tau); & \frac{(2n-1)N}{2n} < i < N-1. \end{cases} \tag{39}$$

where

$$J_i(\tau) = \frac{4\left(\sqrt{1-\tau_i} - \sqrt{1-\tau_{i+1}}\right)}{\pi^2 \sqrt[4]{(1-\tau_i)(1-\tau_{i+1})}} \tan^{-1}\left(\frac{\sqrt[4]{(1-\tau_i)(1-\tau_{i+1})}}{\sqrt{\tau-1}}\right). \tag{40}$$

and

$$x_{1,\beta_i}(\tau) \approx -\frac{1}{\sigma} I_i(\tau)\Upsilon_{k,i}, \quad \tau > 1. \tag{41}$$

Using results (29), (31), (40), (39) and by expanding (25), we get

$$\begin{aligned} x(\tau) \approx & -\frac{1}{\pi}\ln(\tau-1) - \frac{1}{\sigma}\sum_{i=1}^{N/2n} \arccos\left(\frac{L_n}{Nl_i}\right) I_i(\tau)\Upsilon_{k,i}(\tau) \\ & + \frac{1}{\sigma}\sum_{k=0}^{n-1}(-1)^k \sum_{i=(2k+1)N/2n}^{(2k+3)N/2n} \arccos\left(\frac{L_n}{Nl_i}\right) I_i(\tau)\Upsilon_{k,i}(\tau) \\ & - \frac{(-1)^n}{\sigma} \sum_{i=(2n-1)N/2n}^{N-1} \arccos\left(\frac{L_n}{Nl_i}\right) I_i(\tau)\Upsilon_{k,i}(\tau), \quad \tau > 1. \end{aligned} \tag{42}$$

$$y(\tau) \approx 1 + \sum_{i=1}^{N/2n} \arccos\left(\frac{L_n}{Nl_i}\right) J_i(\tau) - \sum_{k=0}^{n-1} (-1)^k \sum_{i=(2k+1)N/2n}^{(2k+3)N/2n} \arccos\left(\frac{L_n}{Nl_i}\right) J_i(\tau), + (-1)^n \sum_{i=(2n-1)N/2n}^{N-1} \arccos\left(\frac{L_n}{Nl_i}\right) J_i(\tau), \quad \tau > 1. \tag{43}$$

4.3 The Relation between the length of straight line segments $\|C_jC_{j+1}\|$ and τ_j

Along C_jC_{j+1} where $q = q_j$, $z_j = l_j e^{-i\beta^*}, j = 1, \ldots, N$, we have

$$\theta = \beta^* = \begin{cases} \beta_j, & \tau_j < \tau < \tau_{j+1}, \quad j = 1, 2, \ldots, N/2n, \\ -(-1)^\alpha \beta_j, & \begin{cases} \tau_j < \tau < \tau_{j+1}, \quad \alpha = 0, \ldots, n-1, \\ j = \frac{(2k+1)N}{2n}, \ldots, \frac{(2k+3)N}{2n}, \end{cases} \\ (-1)^n \beta_j, & \tau_j < \tau < \tau_{j+1}, j = \frac{(2n-1)N}{2n}, \ldots, N. \end{cases} \tag{44}$$

On the other hand, from (14)

$$z_j - z_\infty = -\frac{1}{\pi} \int_{\tau_j}^{\tau_{j+1}} \frac{e^{i\beta^*}}{(1-s)q_j(s)} ds = l_j e^{-i\beta^*}, \tag{45}$$

therefore:

$$l_j = -\frac{1}{\pi} \int_{\tau_j}^{\tau_{j+1}} \frac{1}{(1-s)q_j(s)} ds. \tag{46}$$

Along the solid boundaries, we can approximate q_j by one and for (46), we could obtain:

$$l_j \approx -\frac{1}{\pi} \ln\left(\frac{1-\tau_j}{1-\tau_{j+1}}\right). \tag{47}$$

Consequently,

$$\tau_j \approx 1 - e^{-\pi \sum_{\alpha=1}^{j} l_\alpha}. \tag{48}$$

5 Numerical Results

For a large number of the discretization point N, as N increases, the computed segments C_iC_{i+1} more closely approximate the tangent to the arc between these points, leading to higher accuracy in the numerical solutions, and for all $i = 1, \ldots, N$, the segment C_iC_{i+1} approaches the tangent of the arc between C_iC_{i+1}. Additionally, we also use the previous approximate scheme to calculate the solutions and the free surface profiles for a fixed $\delta(x) = \sin(5x)/2$, $n = 2$ and $N = 1000$ and different values of Weber number σ.

Figure 5 presents the variation of the free surface shape with respect to the Weber number. According to this figure, if the Weber number decreases, the curvature of the free surface decreases accordingly; the reason is because this is a characteristic property of the surface tension effects.

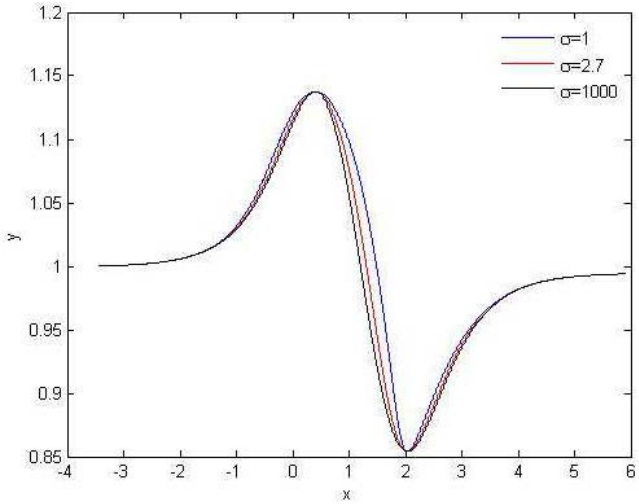

Fig. 5. The effect of Weber number σ on the free-surface profile at a fixed ($\delta(x) = \sin(5x)/2$,$n = 2$ and $N = 1000$.

The free surface profiles for different number of discretization N are plotted in Fig. 6, as N increases, the computed segments C_iC_{i+1} more closely approximate the tangent to the arc between these points, leading to higher accuracy in the numerical solutions. The observed convergence in the free-surface profiles validates the numerical approach, ensuring that $N = 1000$ offers a sufficient resolution for reliable results.

Figure 7 presents the variation of the free-surface profile for different N values at a fixed $\delta(x) = \sin(5x)/2$, $\sigma = 1000$ and $N = 1000$. These variations in N, which determine the shape of the flow field bottom, illustrate the influence of the bottom geometry on the free surface.

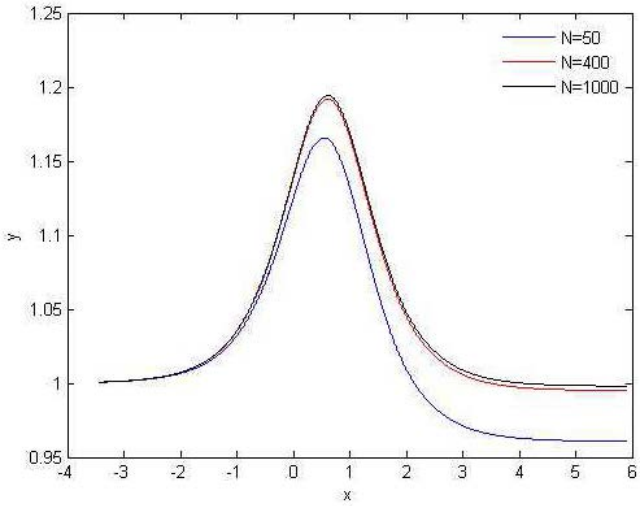

Fig. 6. Effect of the bottom shape on the free-surface profile for different n values and at a fixed $\delta(x) = \sin(5x)/2$, $\sigma = 1000$ and $N = 1000$.

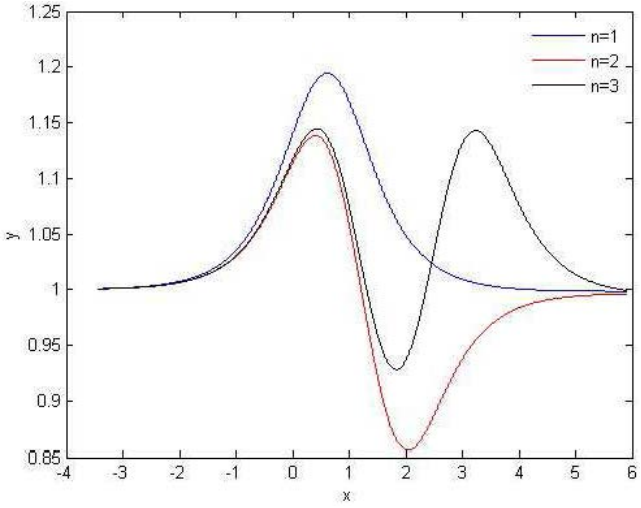

Fig. 7. Effect of number of discretisation point N on the free-surface profile at a fixed $\delta(x) = \sin(5x)/2$, $\sigma = 1000$ and $n = 1$.

6 Conclusion

In this article, we attempted to solve the nonlinear problem of steady free-surface flow over a sinusoidal bottom using a numerical method. The flow domain of the

physical plane was mapped onto an upper half-plane using the Schwartz-Christoffel transformation. The Hilbert method for a mixed boundary value problem resulted in a system of nonlinear integral equations. Additionally, the perturbation technique was employed to approximate the solution for a large Weber number. Illustrations of the results were provided to depict the shape of free surfaces under the influence of the Weber number.

ACKNOWLEDGEMENTS

This paper is supported by the General Direction of Scientific Research and Technological Development (DGRSTD)Algeria...

REFERENCES

[1] G. BIRKOFF, E.H. ZARANTONELLO (1957) "Jet, Wakes and Cavities". Academic, New York.

[2] G.K. BATCHELOR "An introduction to fluid dynamics". Cambridge: Cambridge University Press.

[3] B.K. SHIVAMOGGI (1998) "Theoretical Fluid Dynamics", 2nd Edition,. Wiley-Interscience.

[4] L.M. MILNE-THOMSON (1968) "Theoretical Hydrodynamics", 5th edition. Macmillan, New York

[5] D.E. RUTHERFORD (1959) "Fluid Dynamics". Oliver & Boyd.

[6] L.K. FORBES, L. SCHWARTY (1982) Free-surface flow over a semicircular obstruction. *Journal of Fluid Mechanics* **144** 299–314.

[7] J-M. VANDEN-BROECK (1998) Free-surface flow over an obstruction in a channel. *Physics of Fluids* **30**(8) 2315–2317.

[8] F. DIAS, JOSEPH B. KELLER, J-M. VANDEN-BROECK (1988) Flows over rectangular weirs. *Physics of Fluids* **29** 2071–2076.

[9] M.M. BOUNIF, A. GASMI (2022) An Approximate Solution Technique for the Flow Past an Obstacle with a Large Weber Number. *International Journal of Applied and Computational Mathematics* **8** 1–12.

[10] M.M. BOUNIF, A. GASMI (2021) First order perturbation approach for the free surface flow over a step with large Weber number. *INCAS Bulletin* **13**(2) 11–19.

[11] M.B. ABD-EL-MALEK, S.N. HANNA (1989) Approximate solution of a flow over a ramp for large Froude number. *Computational and Applied Mathematics* **28** 105–117.

[12] J.T.S. KEELER, B.J. BINDER, M.G. BLYTH (2018) Steady two-dimensional free-surface flow over semi-infinite and finitelength corrugations in an open channel. *Physical Review Fluids* **3** 14804.

[13] A. GASMI (2014) Numerical Study of Two-Dimensional Jet Flow Issuing from a Funnel. *Proceedings in Mathematics and Statistics* **87** 161-169.